CHAPTER 6

Basicity of the External Oxo Sites. Dimerisation Reactions

The applications of polyoxometalates are often related to their ability to be protonated. This chapter is aimed at studying a series of Keggin anions protonated at different positions. In section 6.1, the basicity of the oxygen sites of the Keggin framework is studied by means of various methods: qualitatively through the analysis of molecular electrostatic potentials and quantitatively, computing protonation energies at different sites of the external Keggin core. It showed that not all the oxo sites in a POM have the same predisposition to be protonated. The reader shall find a basicity scale for the set of oxo sites in $SiM_3W_9O_{40}$ frameworks, with M = Mo, V and Nb. A phenomenon associated to protonation, the dimerisation of Keggin anions, is studied in deep in sections 6.2 and 6.3. $[SiNb_3W_9O_{40}]^{7-}$ and $[PTiW_{11}O_{40}]^{5-}$ are known to dimerise, and this reaction is investigated to unravel when and how two monomers link to each other. This study is based on the relative protonation energies of different oxo sites in the external metal-oxide core and in the study of some reaction intermediates. The effect of the solvent is taken into account to get realistic reaction energy profiles.

6.1. Basicity of the External Oxygen Sites in Mixed-addenda Keggin Anions

This section is addressed to the study of the basicity of oxo sites in the Keggin anion. For the sake of generality, various compounds are studied, taking the $[SiW_{12}O_{40}]^{4-}$ anion as a reference, and studying various addenda substitutions. The recent history of polyoxometalates has demonstrated that mixed-metal anions are far more interesting than single-addenda ones from the redox and the acid-base properties. Following the same scheme of section 4.2, several $SiM_3W_9O_{40}^{n-}$ clusters are presented and their basicities explored. The vast literature concerning the study of the basicity and the chemistry are a good proof for the importance of this phenomenon. Amongst other chemists, Walter Klemperer performed systematic studies on various types of anions during decades in order to unravel, amongst other features, the chemical properties related to the basicity (or nucleophilicity) of the external oxo sites.[1-14] Klemperer studied functionalised compounds with organic fragments and Ti-derived ligands.

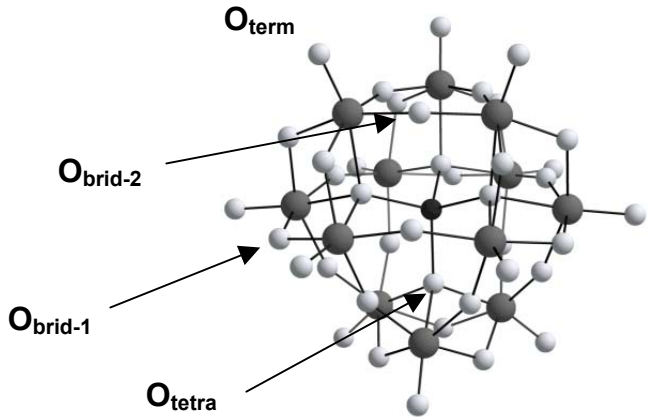

Figure 6.1. Ball-and-stick representation of the single-addenda $SiW_{12}O_{40}^{4-}$ Keggin anion. White spheres represent oxygens, and grey ones metal atoms. The internal dark sphere is the silicon atom. The four oxygen positions are labelled for further discussion.

In single-addenda Keggin anions there are two different external oxo sites, the bridging OM_2 oxygens and the terminal OM ones. In fact, there are two distinct bridging oxygens but, a priori, the differences between them are rather small (Figure 6.1). They are different since those labelled $O_{brid\text{-}1}$ belong to two edge-sharing octahedra, whereas the $O_{brid\text{-}2}$ are shared by corner-sharing MO_6 units. This mere fact leads to differences that will be discussed later. The relative basicity scale of the single-addenda tungstate is not a matter of discussion in this chapter since our interest is centred on mixed-addenda anions. Nevertheless, recent theoretical work performed by Bardin *et al*.[15] and Ganapathy *et al*.[16] analyses this point in the PW_{12} cluster. From these works it arises that bridging oxygens appear to be the most basic at the DFT level. However, the very recent work of Ganapathy *et al*.[16] compares the theoretical results with experimental data, leading to unprecedented conclusions, since they claim from NMR measurements that terminal oxygens could be the first to be protonated.

By removing one or various tungsten centres from the parent SiW_{12} structure and replacing them with different elements we can modify the properties of the cluster. Not only the redox properties or the localisation of the blue electrons are, as we described in section 4.2, but also the surface properties of the POM. This concerns especially the electron density, which is strongly dependent on the intrinsic properties of all the atoms of the framework. The key properties taking part in these changes are the formal charge of the metal centre, its size and the energy of its electronic levels. We will show in the present section how the basicity is affected by the substitution of three Ws by Mo or V. Mo is holding the same formal charge and the size is nearly equivalent, so no great changes are expected in the basicity. Vanadium, on the other hand, is pentavalent and considerably smaller. Both parameters are determinant in the V–O distances and the charge density in the region of substitution, as well. It is worth noting that $SiMo_3W_9O_{40}^{4-}$ has exactly the same charge as the single-addenda SiW_{12}^{4-}. This fact indicates a priori minor changes in the *absolute* basicity after substitution. On the other hand, $SiV_3W_9O_{40}^{7-}$ is highly negatively charged, and its basicity is expected (and well known) to be greater. But the interesting point here is to provide a basicity scale between the different oxo sites of each cluster, having a better approximation to the ordering of protonation in the different sites.

Figure 6.2 shows a three-times-substituted Keggin anion. Notice that the substituted centres belong to corner-sharing octahedra. Addenda metals

in Keggin clusters are more commonly substituted in this fashion. The aim of this section is to contribute to enlarge the knowledge on a well-known family of molecules, to which much effort is invested amongst the experimentalists.

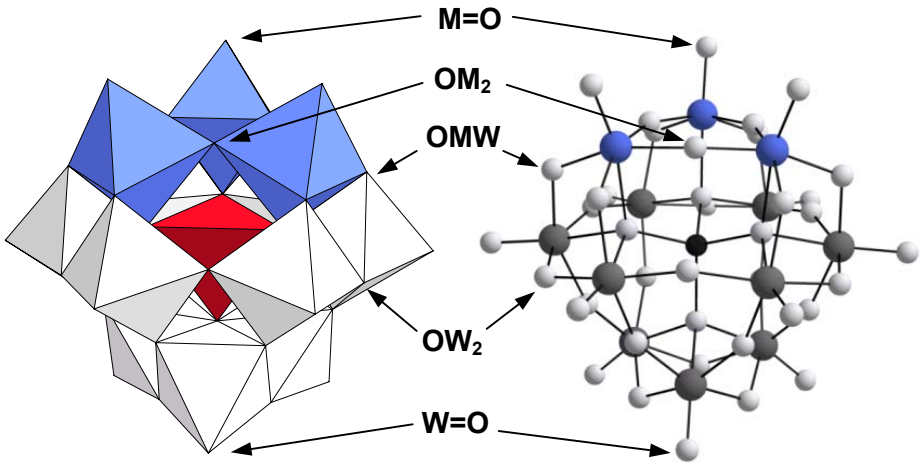

Figure 6.2. Polyhedral and ball-and-stick representation of the mixed-addenda A-α-$SiM_3W_9O_{40}^{n-}$ Keggin anion. The M centres are in blue and grey spheres are the tungsten atoms.

The Keggin structure may be viewed as the assembly of four M_3O_{13} edge-sharing triads (*B-triads*) or as the packing of four M_3O_{15} corner-sharing triads (*A-triads*). Of the lacunary XM_9 units, the anions that contain A-fragments are the most frequent, although many aggregates of the B-XM_9 precursor are also known.[17-19] All the structures reported in the present work are formal derivatives of the Keggin anion: the A-$[SiM_3W_9O_{40}]^{n-}$ species maintain their shape after the substitution. The substitution of a W or a Mo by another metal may modify the charge density throughout the POM and alter the relative basicity of various sites in the molecule. In general, the basicity of the oxygen sites depends on the number of metals linked to the oxo ligand. Hence, for example, experimental[11] and theoretical[20] studies on the decavanadate anion $[V_{10}O_{28}]^{6-}$ showed that the oxygen bonded to three vanadiums is more basic than bridging oxygens and the terminal oxygens are the least basic sites.

Molecular electrostatic potentials

A brief introduction to the electrostatic potential function can be found in chapter 2. From the theoretical point of view, the qualitative study of molecular electrostatic potentials (MESP) proved to be very useful for detecting the most nucleophilic regions of a POM. Electrophilic species —those positively charged— tend to minimise its potential energy by approaching as much as possible a minimum of a MESP distribution. Figure 6.3 shows three views of the MESP distribution on an isodensity 3D-surface for the mixed-addenda anions SiM_3W_9 (M = Mo and V). The colour of the electronic density isosurface (ρ = 0.017 e/ua) in the figure is a function of the MESP value. Red colour identifies regions in which the electrostatic potential is negative (nucleophilic regions) and blue denotes positive or less negative electrostatic potentials (electrophilic regions).

When molybdenums substitute tungstens in SiW_{12}, the electronic reorganisation is quite small and the basicity of the substituted anion is not much different from that of the parent anion. It can be easily deduced from the MESP function that bridging oxygens are generally more basic than terminal oxygens since the regions close to terminal OMo and OW oxygen sites (dark blue) are the least basic. Contrarily, the accessible nucleophilic regions (red) are close to the bridging oxygens. Recall that the more intense red colour —in the vicinity of the internal region— is dominated by the potential of the tetrahedral oxygens, which are the only oxo ligands in the cluster bonded to four positive ions. This oxygen is not easily accessible for a proton, though.

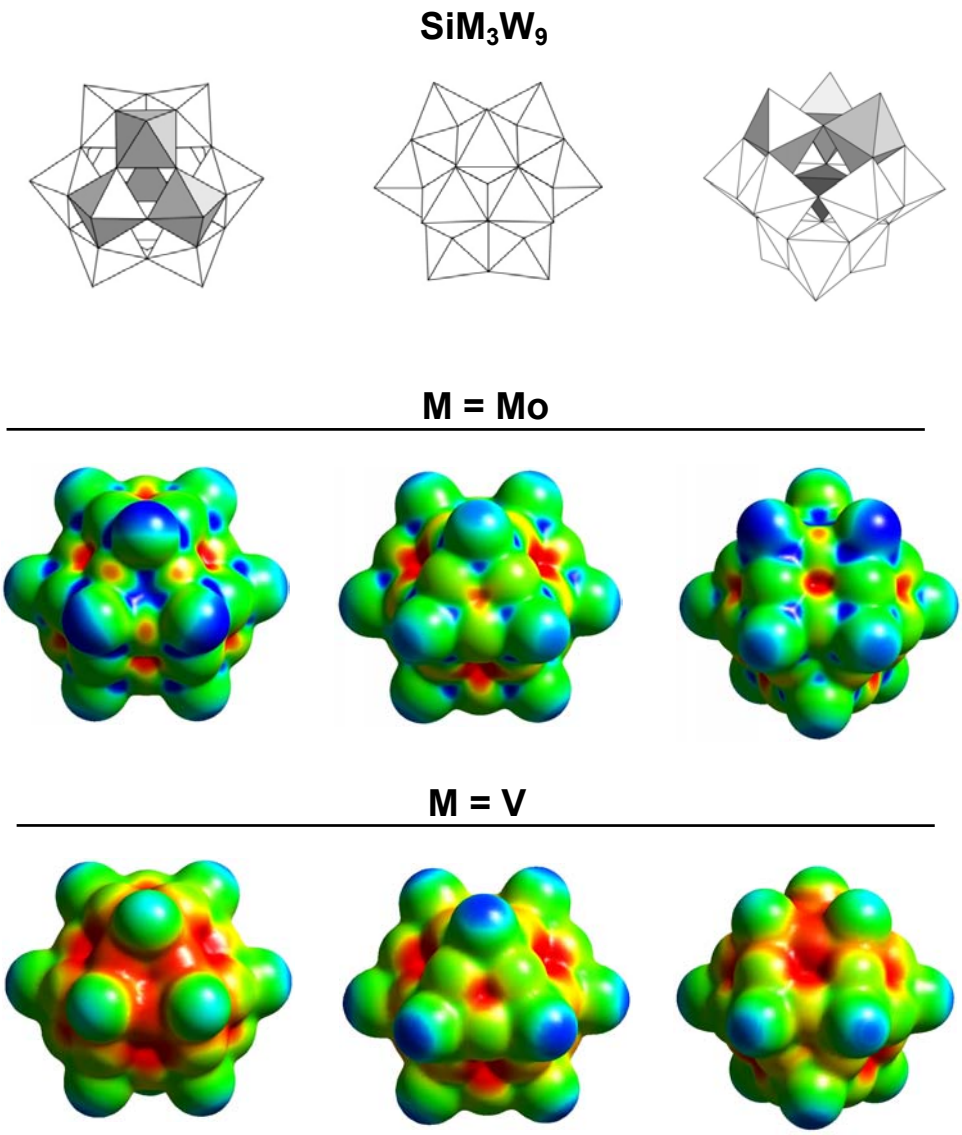

Figure 6.3. Polyhedral representations and Molecular Electrostatic Potentials from three different viewpoints for the $SiMo_3W_9$ and SiV_3W_9 derivatives. See text for further details.

Protonation energies

The qualitative analysis of the MESP just indicated that, on the one hand, the bridging OMo_2 would be the most nucleophilic sites and, on the other, that the terminal OMo oxygen is not a good position for protonation. Computation of the fully optimised structures of the corresponding protonated forms could reinforce this hypothesis. Table 6.1 lists the values of the relative protonation energies for the five isomers H–OM_2, H–OM, H–OW_2, H–OWM, H–OW. The energy sequence matches the qualitative ideas that emanate from the MESP distribution analysis. The most stable protonated complex is the isomer in which the proton is attached to the bridging oxygen linked to two molybdenum ions. The next preferred site is OMoW with a relative energy of only 3.7 kcal mol^{-1} and OW_2 is the least basic of the bridging oxygens and lies at 6.8 kcal mol^{-1}. The energies of H–OMo and H–OW isomers were computed to be 19.8 and15.9 kcal mol^{-1} above the energy

Table 6.1. Relative protonation energies (in kcal mol^{-1}) for all the distinct external oxygens of $[SiM_3W_9O_{40}]^{n-}$, with M = Mo and V. For a better comparison between the two clusters, the zero-energy protonation site was arbitrarily chosen to be OW_2.

M	*Site*	*Relative Energy*
Mo	OMo_2	–4.9
	OMoW	–1.2
	OW_2	0.0
	OW	+11.0
	OMo	+15.0
V	OV_2	–12.4
	OVW	–1.4
	OW_2	0.0
	OV	+5.6
	OW	+19.2

of H–OMo_2, respectively. These results are consistent with the acidity ordering of HPAs, where tungstates are slightly more acidic than molybdates.[21]

It is clear in the MESP distribution of the group 5 SiV_3W_9 derivative (Figure 6.3) that the differences in proton affinity between the most basic and the least basic sites are larger than in W/Mo mixed anions. The blue colour in the vicinity of terminal OW oxygens indicates that these sites might be the least basic ones. In contrast, the wide read area in the region of OV_2 sites is a clear signal that these sites might have the strongest proton affinity. Once again, the calculations carried out on the protonated forms fully confirm the predictions made from MESP since H–OV_2 is the most stable isomer for $HSiV_3W_9$. Our calculations suggest the following basicity scale of the oxo sites in SiV_3W_9: OV_2 > OVW > OW_2 > OV > OW. The difference in the proton affinity between the most and least basic sites is ~30 kcal mol^{-1}. The range is ~10 kcal mol^{-1} wider than in $SiMo_3W_9$.

One proton residing on a bridging oxygen OM_2 with M = W, Mo or V and on a terminal OM has energy differences, according to present DFT calculations, ranging between 9 and 20 kcal mol^{-1}. This is a considerable amount of energy but significantly lower than the 71 kcal mol^{-1} suggested by Davis *et al*. by means of model clusters.[15] These authors, however, performed calculations on triprotonated H_3PM_{12} clusters to determine a reliable proton affinity difference between the bridging oxygens in PMo_{12} and PW_{12} of 9 kcal mol^{-1}. Such a value is fairly similar to the ~6 kcal mol^{-1} computed in the present work for the mixed-addenda $SiMo_3W_9$ cluster. Another important point is that, when the proton attaches to bridging oxygens, there is an additional stabilisation via a weak hydrogen bond with the nearest bridging oxygen. In H–OMo_2, the H–O bond length is 0.99Å and the H···OW_2 distance is 2.03 Å. The conformation with the H oriented outwards from the molecular framework is notably higher in energy, more than 10 kcal mol^{-1}. This additional stabilisation is similar in H–OMo_2 and H–OW_2 and, therefore, does not modify their relative stability, but it is an important factor in the difference of affinity between a proton residing on a terminal and in bridging oxygen. The important stabilisation energies computed in protonated clusters with H···O bonds account for the importance of this weak interaction. Notably, Keggin anions protonated at terminal M=O bonds do not allow H···O bond formation, thus they remain higher in energy. See Figure 6.4 for a visualisation of the interactions.

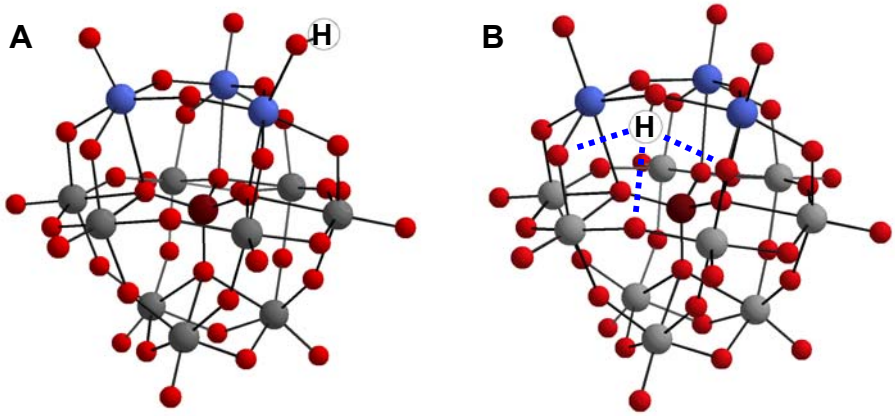

Figure 6.4. SiM_3W_9 model clusters protonated at a (A) terminal or a (B) bridging oxo site. White spheres are hydrogen atoms. Notice the H···O stabilising interactions in the latter case.

6.2. Dimerisation Processes in Mixed-addenda Keggin Anions

Introduction

The acid-base properties in POMs have been deeply investigated in history with the aim of exploiting their associated features. One of them is the inclusion of POMs in reactions acting as catalysts. Many experimental works have shown that the likeliness of a Keggin anion to be protonated is strongly dependent on its chemical composition. Furthermore, different oxo sites in the metal-oxide core of POMs have different affinity to protons, so POM chemists have learnt to vary composition and structure to tune the properties.

In the middle 80's, the first successful attempts to obtain a Keggin dimer were reported by Richard G. Finke[22] and Walter G. Klemperer.[10-23] Even though, the dimerisation and the rules governing this reaction are not fully understood since serious difficulties are found to elucidate intermediate species. Nevertheless, valuable experimental hints are available concerning the capability of the external oxo sites to be protonated in POMs. In this section we analyse and discuss the relationship existing

between the basicity in Keggin anions and the dimerisation processes. It is well known that the synthesis of mixed-addenda anions led to the possibility of discovering new ways of assembly, in which the physical nature of the substituting metal element plays a fundamental role.

In the single-addenda Keggin tungstate, a protonation at the terminal W=O site is very unfavourable since the bridging OW_2 oxygen is notably more basic. Even though, the presence of other metals, M, in the framework ($XM_xW_{12-x}O_{40}$) can modify the relative basicity of the oxygen sites, favouring the protonation at regions close to the substituted metal. Many mixed-addenda Keggin structures have been synthesised and characterised,[24-25] but only derivatives containing Nb, Ti and Cr dimerise to form M–μ-O–M unions,[22-27] indicating that the nature of M is very important (see Figure 6.5).

This section is devoted to the study of two monomeric systems and their dimeric partners as well as the reaction pathways of dimerisation. $PTiW_{11}O_{40}^{5-}$ and $SiNb_3W_9O_{40}^{7-}$ are known to dimerise under suitable conditions. First of all, the data related to the basicity of the various relevant oxo sites is presented for both clusters. Afterwards, the reader shall find possible dimerization pathways for the Ti- and Nb-derivatives. All the calculations presented take into account solvent effects since the relative energy of the species considered is of much importance. The solvent is considered by means of a continuum model as implemented in the COSMO method.[28] See chapter 8 for details.

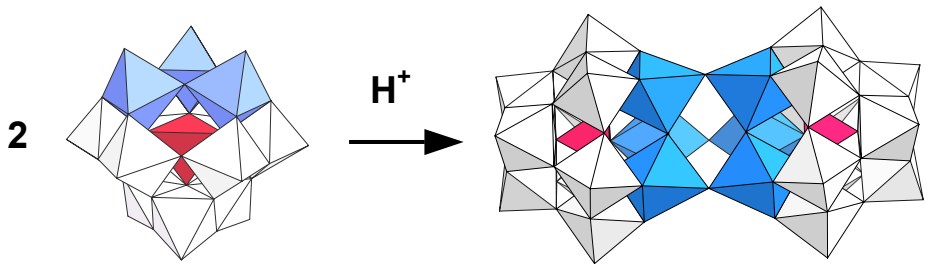

Figure 6.5. Polyhedral representation of a generic dimerisation reaction to form the $X_2M_6W_{18}$ anion. Blue octahedra contain the M centres.

6.2.1. Dimerisation of $PTiW_{11}O_{40}^{5-}$

In 2000, Kholdeeva *et al*.[27] reported the dimerisation of the monosubstituted Ti-derivative of the Keggin anion. It was achieved under acidic conditions and a single M–μ-O–M linkage was formed. From subsequent characterisation, it was found to be a Ti–O–Ti bridge and the overall yield was of 98% conversion. This dimer exhibited catalytic properties in the presence of H_2O_2. Contrarily, the monomer did not have so much activity. Other titanopolytungstates have been found to catalyse oxidation reactions of thioethers with hydrogen peroxide[29] in nearly quantitative yield.

The authors of that study assumed that protonation occurs at the Ti=O site prior to Ti–O–W. Even though, no strong evidence of the compounds formed at intermediate steps of the process is yet available. The aim of this section is to present the DFT results obtained on the protonation of the monomer and the reaction pathway to form the dimer $(PTiW_{11}O_{39})_2(\mu\text{-OH})$ from the monomer $PTiW_{11}O_{40}$. Figure 6.6 shows a schematic view of the dimerisation reaction for $PTiW_{11}$.

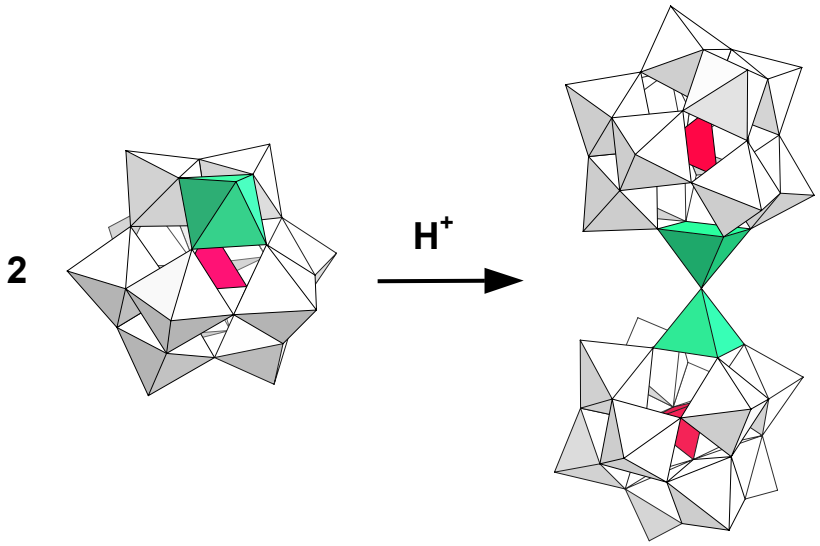

Figure 6.6. Polyhedral representation of the monomeric $PTiW_{11}$ and the dimeric $(PTiW_{11})2(\mu\text{-O})$ forms discussed in this section. Green polyhedra contain the titanium atoms.

Basicity of the oxo sites in $PTiW_{11}O_{40}^{5-}$

The dimerisation reaction starts with the protonation of $PTiW_{11}$. The detailed analysis of the most basic sites of the monomer is performed, as in section 6.1, determining the MESP distribution and the protonation energies at different sites. A 3D representation of the MESP function (Figure 6.7) shows a high proton affinity in the vicinity of the external oxygen of the octahedron that contains the Ti^{4+}. The bridging OTiW sites appear as competitive nucleophilic sites, whereas the next most basic sites are the bridging oxygens bonded to two tungstens. As previously described for other mixed-addenda systems, the terminal W=O atoms are the least basic sites.

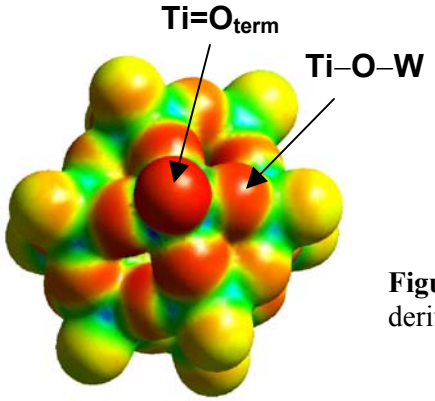

Figure 6.7. MESP for the $PTiW_{11}$ derivative.

Table 6.2. Protonation energies computed (kcal mol^{-1}) for $PTiW_{11}$. Note the effect of the introduction of a solvent in the relative protonation energies.

Protonation Site	*Gas phase*	*Acetonitrile*
OW_2	0.0	0.0
OTiW	–2.9	–2.2
OTi	–8.5	–13.1

Assuming that the Ti=O, OTiW and OW_2 are the most basic sites, the geometries for the three corresponding protonated isomers were fully optimised. According to the MESP distribution, the cluster with the proton bonded to the Ti=O oxygen is the most stable. Table 6.2 shows that

protonation at the bridging OTiW site is 5.6 kcal mol^{-1} less favourable, energy that increases up to 11.4 kcal mol^{-1} in a solution of acetonitrile (dielectric constant of 37.0).

The additional relative stabilisation of the Ti=OH form is attributed to a more efficient interaction between the proton and the solvent in this isomer. The inward orientation of the proton when it is linked to a bridging site does not favour its stabilisation by electrostatic interaction with the solvent molecules. So, the qualitative analysis through the electrostatic potential function and the relative protonation energies coincide, reinforcing the experimental assumption that the Ti=O site is the most basic on the Ti-derivative.

Dimerisation pathways

According to the scheme proposed by Kholdeeva *et al.*,[27] the formation of the dimer $(PTiW_{11}O_{39})_2O$ occurs after protonation of the monomer $PTiW_{11}O_{40}$ at the terminal Ti=O site. Then, two protonated molecules $HPTiW_{11}O_{40}$ react to give the dimer. The reaction could also start from H–OTiW, the second protonated monomer in stability. The next step in both cases would be the loss of a water molecule to give $(PTiW_{11}O_{39})_2(\mu\text{-}O)^{8-}$. This cluster has been also observed in its protonated (μ-OH) form. The plausible mechanism for the formation of the dimer may be described, therefore, by the next four equations

Chart 6.1

$$2\,[PTiW_{11}O_{40}]^{5-} + 2\,H^{+} \longrightarrow 2\,H[PTiW_{11}O_{40}]^{4-} \quad (1)$$

$$2\,H[PTiW_{11}O_{40}]^{4-} \longrightarrow H_2[(PTiW_{11}O_{39})_2(\mu\text{-}O)_2]^{8-} \quad (2)$$

$$H_2[(PTiW_{11}O_{39})_2(\mu\text{-}O)_2]^{8-} \longrightarrow [(PTiW_{11}O_{39})_2(\mu\text{-}O)]^{8-} + H_20 \quad (3)$$

$$[(PTiW_{11}O_{39})_2(\mu\text{-}O)]^{8-} + H^{+} \longrightarrow [(PTiW_{11}O_{39})_2(\mu\text{-}OH)]^{7-} \quad (4)$$

The product of step 2 will be different depending on the protonation site of the monomer. If the reaction starts with the protonation at Ti=OH, the intermediate III-1 is formed, but if the protonation at the bridging OTiW oxygen happens, III-2 is the intermediate (Figure 6.8). Step 2 is shown in more detail in Chart 6.2. A great computational effort was made to fully optimise all reactants, intermediates and products involved in the reactions in Chart 6.1.

Chart 6.2

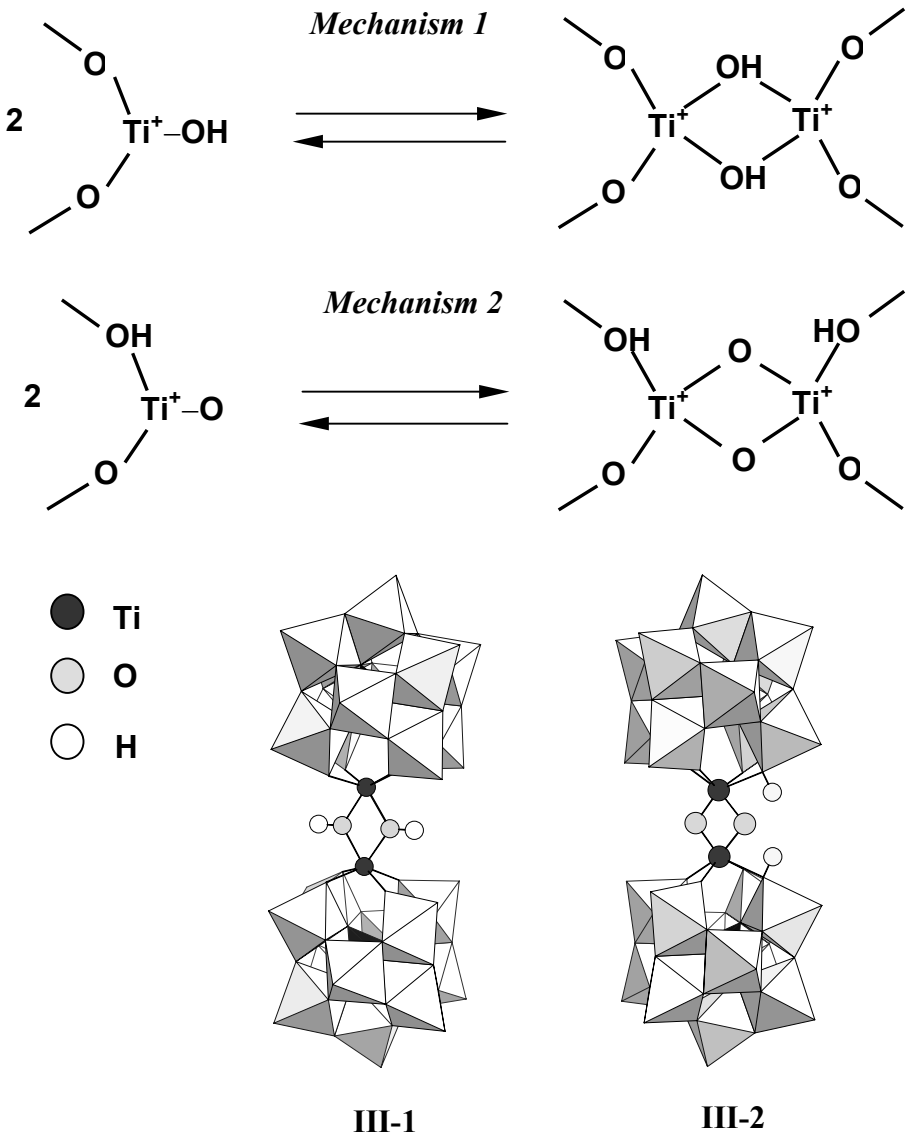

Figure 6.8. Polyhedral view of intermediates III-1 and III-2. They are associated to mechanisms 1 and 2, respectively.

The energy profiles associated to pathways 1 and 2 are represented in Figures 6.9 and 6.10. The energies correspond to single-point calculations of the molecules in acetonitrile media (ε = 37.0). The energies of all points are referred to that of point I, which is the same in both pathways. Labels I, II-1, II-2, III-1, etc. denote monomers, intermediates and dimers involved in reactions 1-4. The reader, however, must take in mind that the energy for points I-V in Figures 6.9 and 6.10 were computed taking into account all the species necessary for charge and matter conservation (Chart 6.3).

Chart 6.3

Pathway 1

I: 2 $PTiW_{11}O_{40}^{5-}$ + 3 H_3O^+

II-1: 2 $[P(TiOH)W_{11}O_{39}]^{4-}$ + H_3O^+ + 2 H_2O

III-1: $[(PTiW_{11}O_{39})_2(\mu\text{-}OH)_2]^{8-}$ + H_3O^+ + 2 H_2O

IV: $[(PTiW_{11}O_{39})_2\mu\text{-}O]^{8-}$ + H_3O^+ + 3 H_2O

V: $[(PTiW_{11}O_{39})_2\mu\text{-}(OH)]^{7-}$ + 4 H_2O

Pathway 2

I: 2 $PTiW_{11}O_{40}^{5-}$ + 3 H_3O^+

II-2: 2 $[HPTiW_{11}O_{40}]^{4-}$ + H_3O^+ + 2 H_2O

III-2: $H_2[(PTiW_{11}O_{39})_2(\mu\text{-}O)_2]^{8-}$ + H_3O^+ + 2 H_2O

IV: $[(PTiW_{11}O_{39})_2\mu\text{-}O]^{8-}$ + H_3O^+ + 3 H_2O

V: $[(PTiW_{11}O_{39})_2\mu\text{-}(OH)]^{7-}$ + 4 H_2O

From the energy profiles in Figures 6.9 and 6.10 is clear that the overall process is quite exothermic, since the reaction products IV and V are about 50 kcal mol^{-1} more stable than the reactants. Another significant fact is that the initial step is also very exothermic (–49.7 kcal mol^{-1}) when the protonation occurs at Ti=O (pathway 1). However, the formation of III-1 requires a significant amount of energy (~25 kcal mol^{-1}). Contrarily, the protonation at OTiW is less stabilising (–28.0 kcal mol^{-1}) and intermediate III-2 is quite high in energy (–4.9 kcal mol^{-1}). Figure 6.11 compares the

energy profiles associated to pathways 1 and 2. This plot clearly indicates that dimerisation of the mixed-addenda Ti-derivative should occur mostly through protonation at Ti=O and formation of III-1. To sum up, present calculations strongly suggest that the major basicity of the terminal Ti=O oxygen site determines the mechanism of dimerisation.

Table 6.3 shows computed distances and angles for the species involved in the dimerisation of the Ti-derivative. Only parameters of the local region of linkage between monomers are listed since the rest of the molecule does not change with regard to the monomer. Notice the enlargement of the Ti···Ti distance when forming the protonated dimer (V) and the great difference between intermediates III-1 and III-2 in the region of linkage. The formation of Ti–μ-(OH)–Ti shortens the Ti···Ti distance by more than 0.5 Å.

Table 6.3. Selected distances (in Å) and angles for the Ti-species involved in points I–V of pathways 1 and 2 of dimerisation.

		III-1	III-2	IV	V
distance					
	Ti···Ti	3.53	2.97	3.69	4.07
	Ti–(μ-O)	2.06	1.92	1.85	2.06
	P···Ti	3.94	4.24	3.68	3.57
	(μ-O)–H	0.98	–	–	0.98
angle					
	Ti–(μ-O)–Ti	108.4	105.7	179.5	161.6

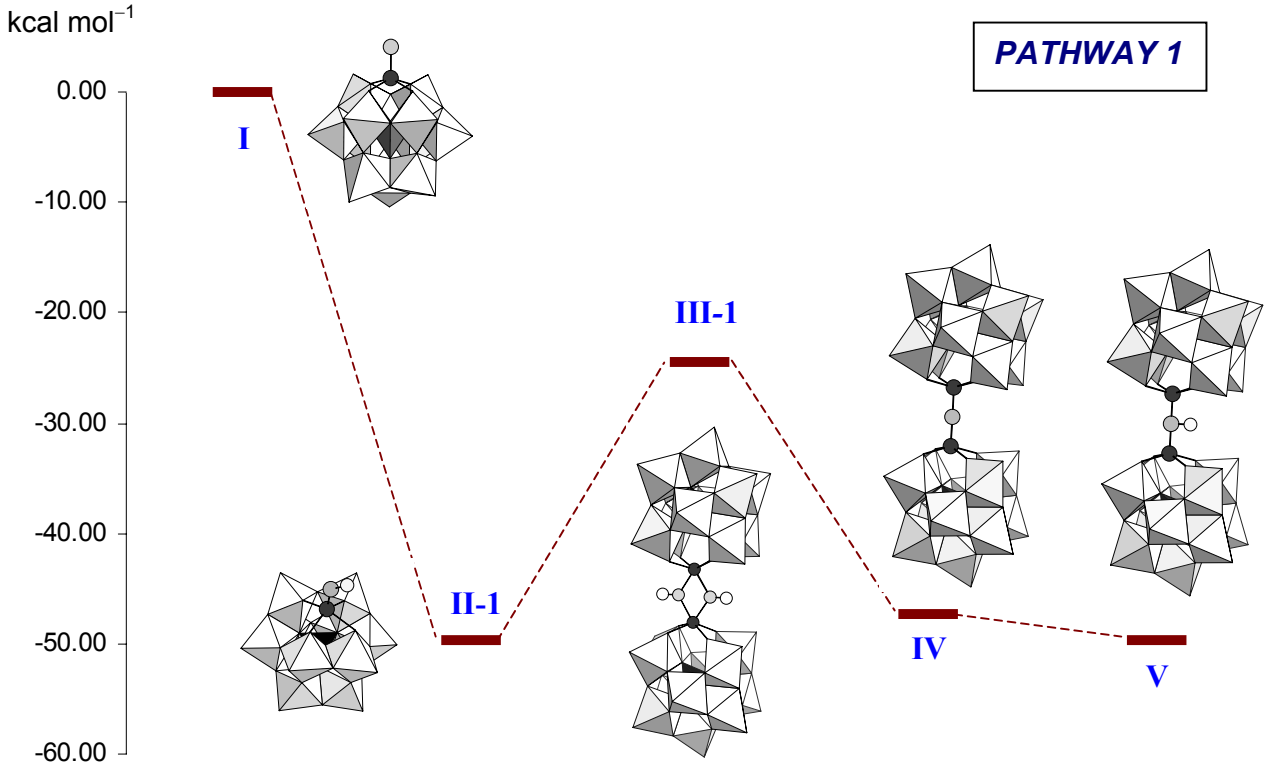

Figure 6.9. Reaction energy profile computed for pathway 1 of formation of $(PTiW_{11}O_{39})OH^{7-}$. Each point I-V contains all the necessary chemical species for charge and matter conservation. See Chart 6.3 for a detailed description of each point.

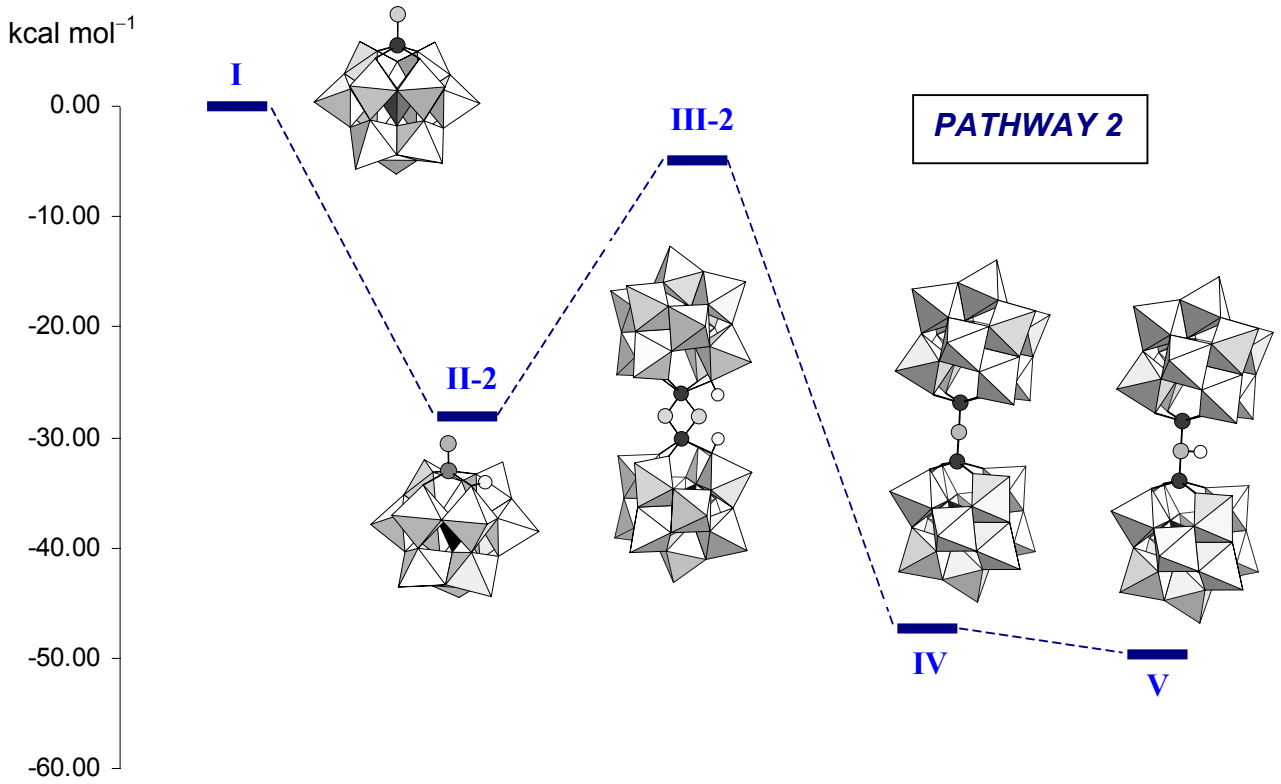

Figure 6.10. Reaction energy profile for pathway 2. Intermediates II-2 and III-2 are different from pathway 1, whereas species I, IV and V are equivalent to the homologous species in Figure 6.9.

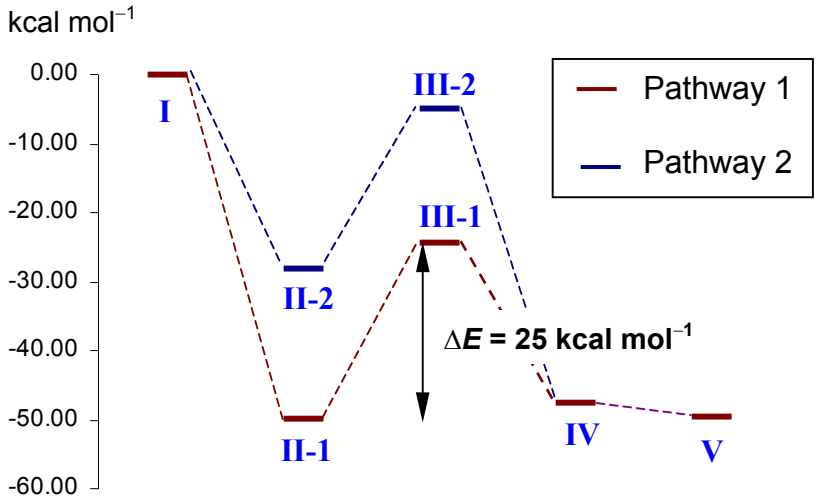

Figure 6.11. Combined reaction profiles for pathways 1 and 2 for the dimerisation of $PTiW_{11}$.

6.2.2. Dimerisation of $SiNb_3W_9O_{40}^{7-}$

The synthesis of $(SiNb_3W_9O_{37})_2O_3^{8-}$ reported by Finke *et al.*[22] in 1984 was the landmark work on the formation of Keggin dimers. That work opened a novel class of reactions in HPAs. Later studies related to the dimerisation reaction of Keggin clusters have been reported.[26d-e] Very recently, Weinstock and co-workers addressed an exhaustive study about the formation of Nb–μ-O–Nb bonds.[30] The authors report pH-controlled reversible and stepwise formation of individual linkages. The monomer, $SiNb_3W_9$, and the dimer, $Si_2Nb_6W_{18}$, are represented in Figure 6.5.

This subsection presents the results about the formation of the Nb–μ-O–Nb linkage in Nb-substituted Keggin anions. The study is conducted in the same fashion as section 6.2.1, dealing with data from MESP, protonation energies and, finally, the reaction energy profile.

Basicity of the oxo sites in $SiNb_3W_9O_{40}^{7-}$

The case of $SiNb_3W_9$ is slightly different from that of the monosubstituted Ti-derivative. In the present anion, three neighbouring Nb atoms form a corner-sharing triad, so three Nb–O–Nb bridging oxygen sites link the niobium centres. These oxygens are supposed to be rather basic since the excess of negative charge of the cluster is somewhat concentrated in the region of substitution. The electrostatic potential function showed in Figure 6.12 supports this statement. Blue regions are localised around terminal W=O oxo sites, which are, *a priori*, the least basic in this anion. From the MESP, other sites competing with ONb_2 for an incoming H^+ could be ONbW and Nb=O, as well.

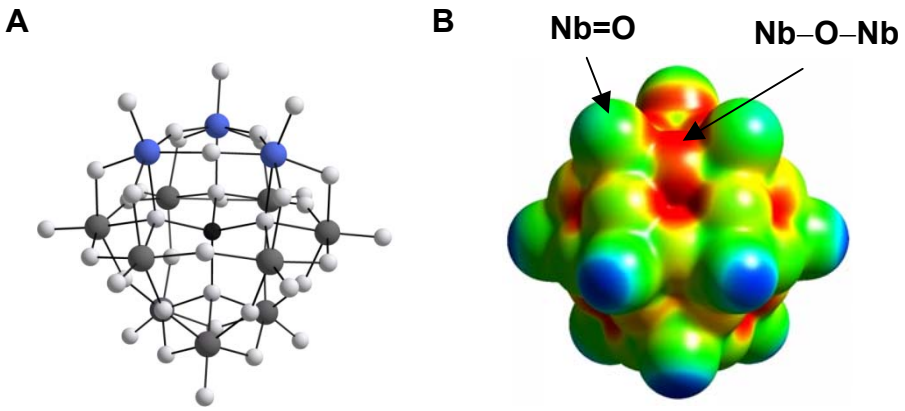

Figure 6.12. (A) Ball-and-stick view of $SiNb_3W_9$ (blue spheres are Nb atoms), and (B) MESP plotted in colour over an isodensity surface of $SiNb_3W_9$.

The relative energies computed for the most suitable isomers of $HSiNb_3W_9^{6-}$ is listed in Table 6.4. The Nb–O–Nb oxygen is the most basic, followed by the terminal Nb=O site in acetonitrile media. The effect of the solvent favours the stabilisation of the most exposed protons like in preceding examples. We assume that protonations at W=O oxygen sites are much higher in energy and they would not attach the proton preferentially.[31]

Table 6.4. Relative protonation energies (in kcal mol^{-1}) of $SiNb_3W_9$ at three oxo sites, computed in the gas phase and in a solvent (ε = 37) with the COSMO program.

Protonation Site	*Gas phase*	*Solvent*
OW_2	0.0	0.0
ONb_2	−11.5	−7.8
ONb	+3.6	−4.4

Data concerning the protonation energies reinforce the fact that this cluster behaves rather differently from $PTiW_{11}$. Now, the competition between ONb_2 and Nb=O for the proton is possible. The energies of protonation between these two sites only differ in 3.4 kcal mol^{-1}, which is a small value. In a series of papers, Klemperer's group studied the reactivity of the $Nb_2W_4O_{19}^{4-}$ Lindqvist anion,[4,10,13-14] concluding that the ONb_2 site is the most basic, nucleophilic oxo site. From a Hartree–Fock study, Maestre *et al*.[32] found the same trend for the basicity of the external oxygens of that Nb-derivative.

Dimerisation pathways

The case we deal with in this section is somewhat more complex because three μ-O bridges are ready to be formed in a stepwise process.[30] For the sake of simplicity, we will only discuss here the formation of a single μ-O bridge between two monomeric units for analogy with the case of the Ti-derivative. For this purpose, the energies in solution were computed for the monomer, the protonated monomer and two reaction intermediates as well as the product of reaction, $(SiNb_3W_9)_2(\mu\text{-}O)$.

Let us take into account again the mechanisms showed in Chart 6.2. If we replace Ti by Nb in that scheme, equivalent intermediates are formed, but in the present case are labelled as VIII-1 and VIII-2. We represent these two species in Figure 6.13 in polyhedral view.

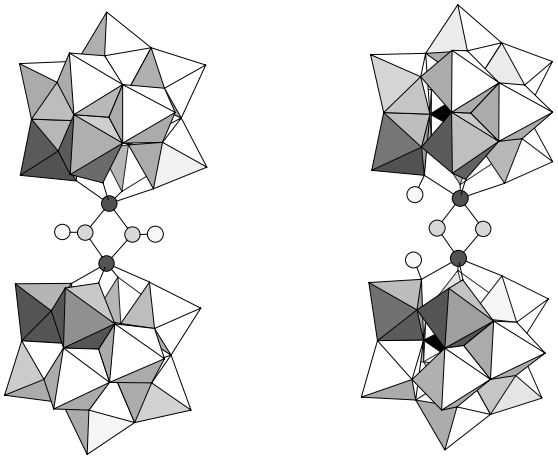

Figure 6.13. The two intermediates, VIII-1 (left) and VIII-2 (right), participating in the formation of the first μ-O bridge in the dimerisation of $SiNb_3W_9O_{40}^{7-}$. Dark polyhedra and dark spheres contain the Nb centres. Light grey spheres represent oxygens, and the white ones hydrogens.

The formation of $(SiNb_3W_9)_2\mu$-O might occur through these two intermediates. At each stage the following species are present:

Chart 6.4

Pathway 1

VI: 2 $[SiNb_3W_9O_{40}]^{7-}$ + 3 H_3O^+

VII-1: 2 $[Si(NbOH)Nb_2W_9O_{39}]^{6-}$ + H_3O^+ + 2 H_2O

VIII-1: $[(SiNb_3W_9O_{39})_2(\mu\text{-}OH)_2]^{12-}$ + H_3O^+ + 2 H_2O

IX: $[(SiNb_3W_9O_{39})_2\mu\text{-}O]^{12-}$ + H_3O^+ + 3 H_2O

Pathway 2

VI: 2 $[SiNb_3W_9O_{40}]^{7-}$ + 3 H_3O^+

VII-2: 2 $[HSiNb_3W_9O_{40}]^{6-}$ + H_3O^+ + 2 H_2O

VIII-2: $H_2[(SiNb_3W_9O_{39})_2(\mu\text{-}O)_2]^{12-}$ + H_3O^+ + 2 H_2O

IX: $[(SiNb_3W_9O_{39})_2\mu\text{-}O]^{12-}$ + H_3O^+ + 3 H_2O

The energy profiles for both pathways of dimerisation (Figure 6.14) show that the step of protonation (VI → VII) of the monomer is quite exothermic (more than 50 kcal mol^{-1}). Point VII of reaction is slightly more stable for pathway 2 by about 7 kcal mol^{-1}, as has been showed in the study of the relative basicity of $SiNb_3W_9$ oxo sites. The formation of intermediates VIII-1 and VIII-2 from their protonated monomers is very endothermic, though. After the second step, species VIII-1 turns to be the most stable by ~12.6 kcal mol^{-1} at this point of the reaction, which implies a crossing of both profiles in step 2. The energy difference at point VIII is moderate between both pathways. So, the intermediate species formed by two μ-(OH) linkages is again the most stable. This may indicate that the protonation at Nb=O (first step of reaction), although being less favoured, is more willing to yield the product dimer than the $H–ONb_2$ form.

In the last step, intermediates VIII-1 and VIII-2 lose a H_2O molecule to give the dimer IX. The energy loss is only 4.1 kcal mol^{-1} for pathway 1, and 16.7 kcal mol^{-1} for pathway 2. The energy of IX, in relation to VI, is –5.9 kcal mol^{-1}. We attribute this small exothermicity to the high negative charge (−12) of the final product.

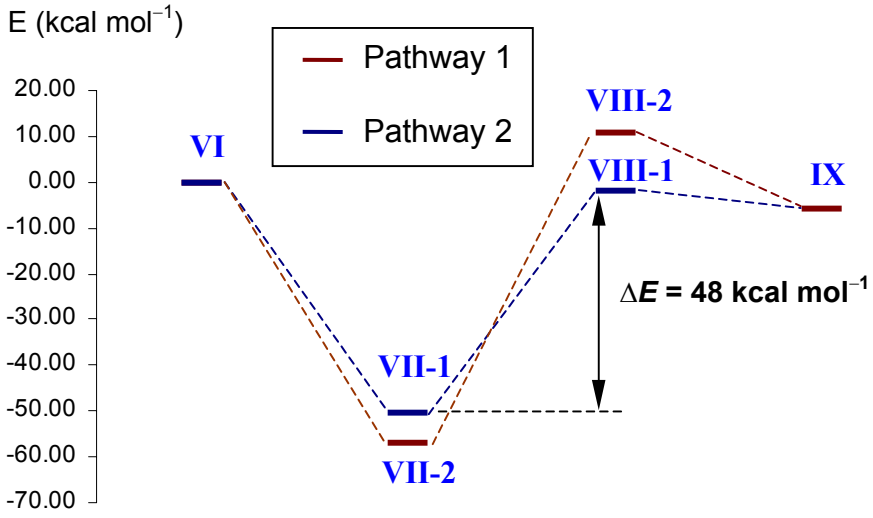

Figure 6.14. Combined energy profiles for pathways 1 and 2 for dimerisation of $SiNb_3W_9$.

Table 6.5 shows computed parameters for the species involved in the dimerisation of the Nb-derivative. These geometric data correspond to the region of formation of the μ-O linkage. The regions far from the Nb centres remain fairly unchanged. The Si···Nb_1 distance changes notably from the monomeric forms, VI-VII, to the dimerised species. In the former cases, it was computed to be 3.70 Å, whereas, as shown in the table, it becomes 4.12 Å for the final dimer. Neither the Si···Nb_2 nor the Nb_2···Nb_2 distances change appreciably.

Table 6.5. Selected distances (in Å) and angles for the Nb-species involved in points VI–IX of pathways 1 and 2 of dimerisation.

	VIII-1	VIII-2	IX
distance[a]			
Nb_1···Nb_1	3.95	3.31	4.09
Nb_1–(μ-O)	2.26	2.00	2.05
Si···Nb_1	4.17	4.44	4.12
Si···Nb_2	3.70	3.66-3.75	3.70
Nb_1···Nb_2	3.83	3.92-4.23	3.82
Nb_2···Nb_2	3.77	3.77	3.78
(μ-O)–H	0.98	–	–
angle			
Nb-(μ-O)-Nb	121.5	106.5	175.8

a) Nb_1 is the centre directly bonded to μ-O, whereas Nb_2 are the neighbouring atoms.

In more acidic conditions, the remaining Nb=O sites are protonated and the di-μ-O bridged dimer $[Si_2Nb_6W_{18}O_{78}]^{10-}$ and the tri-μ-O $[Si_2Nb_6W_{18}O_{77}]^{8-}$ dimer are formed. The complete reaction is accomplished following the process:

$$2\ [SiNb_3W_9O_{40}]^{7-} + 6\ H_3O^+ \rightarrow [(SiNb_3W_9O_{37})_2(\mu\text{-}O)_3]^{8-} + 9\ H_2O$$

It is worth noting that the formation of the three Nb–μ-O–Nb linkages is highly exothermic, $\Delta E = -158$ kcal mol^{-1}. This value contrasts with the

stabilisation found for the mono-μ-O dimer, –5.9 kcal mol^{-1} (Figure 6.14). We believe that this difference in stability originates in the different charges of the clusters. Although in a POM the total charge is stabilised by the solvent, the anions with larger charges gain stability if they transform to less charged clusters. Therefore, this energetic behaviour would explain why the tri-μ-O dimer is found preferentially. Thus, for obtaining the mono- or di-μ-O dimers, the pH conditions must be carefully controlled.[30] From present discussion we wonder whether the simple substitution of the central Si atom by P in XNb_3W_9 would favour the self-assembly of the cluster because in this case the charge of the mono-μ-oxo dimer would be –10 instead of –12. Finally, another question remains still open: why the $XV_3W_9O_{40}^{n-}$ anions do not dimerise? We believe that the strong difference in the basicity of terminal V=O and OV_2 oxygen sites could be the responsible. Calculations are underway to solve this puzzle question.

Table 6.6 lists computed geometrical parameters for the tri-μ-O dimer that are in excellent agreement with the available X-ray data.[26d]

Table 6.6. Selected computed and experimental distances (in Å) and angles for the $[(SiNb_3W_9O_{37})_2(\mu\text{-}O)_3]^{8-}$ dimer.

	Calculated	Experimental[a]
distance[a]		
$Nb_1\cdots Nb_2$[b]	3.67	3.55
$Nb_1\cdots Nb_1$[c]	3.77	–
Nb–(μ-O)	1.95	1.91
Si···Nb	3.50	–
Nb···O	1.95	–
angle		
Nb-(μ-O)-Nb	140.2	137.0

a) X-ray averaged parameters from the crystal structure of reference 26d.
b) Nb_1 and Nb_2 correspond to two Nb centres linked through a μ-O site.
c) Two Nb_1 centres are neighbours in the same Keggin unit.

Finally, we remark that no significant electronic differences were found between the dimers and the corresponding monomers. Hence, the HOMO-LUMO gap in $[(PTiW_{11}O_{39})_2(\mu\text{-}OH)]^{6-}$ and both the mono- and tri-μ-O Nb-dimers is almost identical to that determined for the monomers. This means that the differences in the redox properties between the monomers and dimers would originate exclusively in the whole charge of the cluster.

6.3. Basicity of the $PTi(O_2)W_{11}O_{39}^{5-}$ Peroxo Derivative

A DFT study of the mixed-addenda $[PTi(O_2)W_{11}O_{39}]^{5-}$ (**1**) peroxo derivative was performed to identify the most basic site of this anion in collaboration with Kholdeeva *et al*.[33] The unprotonated and various protonated clusters were computed. This study is aimed at characterising this species, which possesses catalytic activity. The selective catalytic oxidation of organic compounds with an environmentally attractive oxidant, aqueous H_2O_2, is of both academic and industrial interest.[34]

Conclusions concerning the structure of **1** based on the experimental findings are supported by DFT calculations performed for $[PTi(O_2)W_{11}O_{39}]^{5-}$ and its protonated partner. To obtain the geometry of minimal energy for the non-protonated complex, three orientations of the peroxo group were explored for the $[PTi(O_2)W_{11}O_{39}]^{5-}$ anion. Two orientations were computed under the restrictions of the C_s point group, labeled **2a** and **2b** in Chart 6.5 (their relative energies are indicated in kcal mol^{-1}), one of them with the σ-plane containing the Ti center and the O_2 group (**2a**), and the other one with the peroxo group perpendicular to σ (**2b**). Both conformations are very similar in energy, only differing by a mere 1.15 kcal mol^{-1}. The third structure, **2c**, of C_1 symmetry in which the peroxo group is almost aligned with the Ti–O–W plane, is clearly more stable (6–7 kcal mol^{-1}) than the conformations where the O_2 ligand is rotated ~45º with respect to the eclipsed conformation.

Chart 6.5

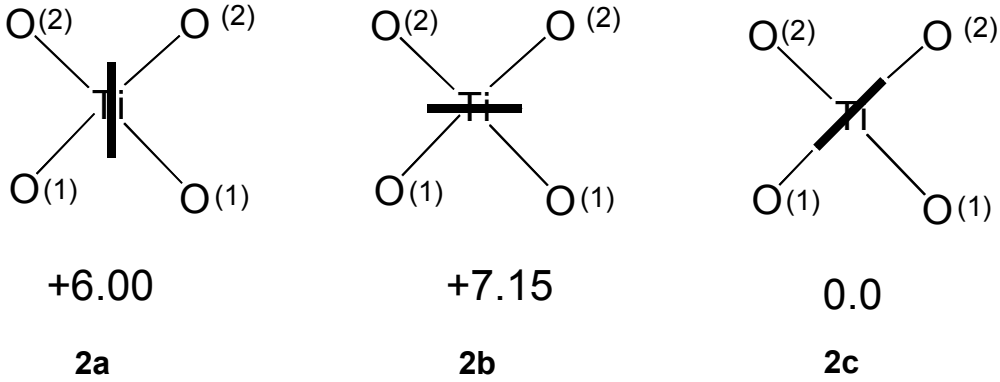

The latter orientation permits electron donation from the occupied π^*_{O-O} orbital to the vacant d_{xy}(Ti)-like orbital by in-phase π^*-d overlapping (Figure 6.15). Such an effect produces an extra stabilisation of the HOMO of the **2c** form, being 0.3–0.4 eV lower in energy than in the *alternated* homologues (Figure 6.16).

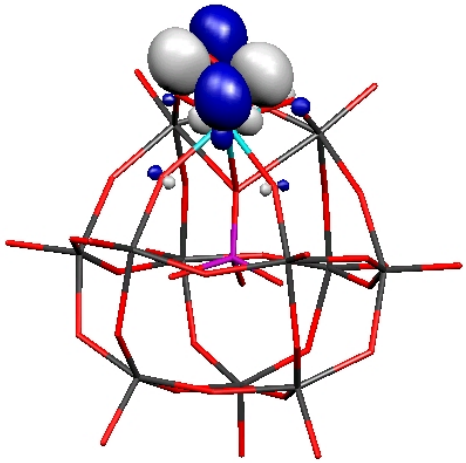

Figure 6.15. Representation of the HOMO for the eclipsed peroxo form **2c**.

The bond lengths computed for O–O and O–Ti in the most stable eclipsed conformation are 1.50 and 1.90 Å, respectively. It is worth

mentioning that POM geometries are very well reproduced by DFT methods, with average deviations from X-ray data of about 0.03 Å.[35-37] The only exception corresponds to the metal-terminal oxygen distances, which are in general, overestimated by ~0.05 Å. The O(1) oxygens link the TiW_2 triad with another triad whereas O(2) are bridging oxygens inside the TiW_2 triad.

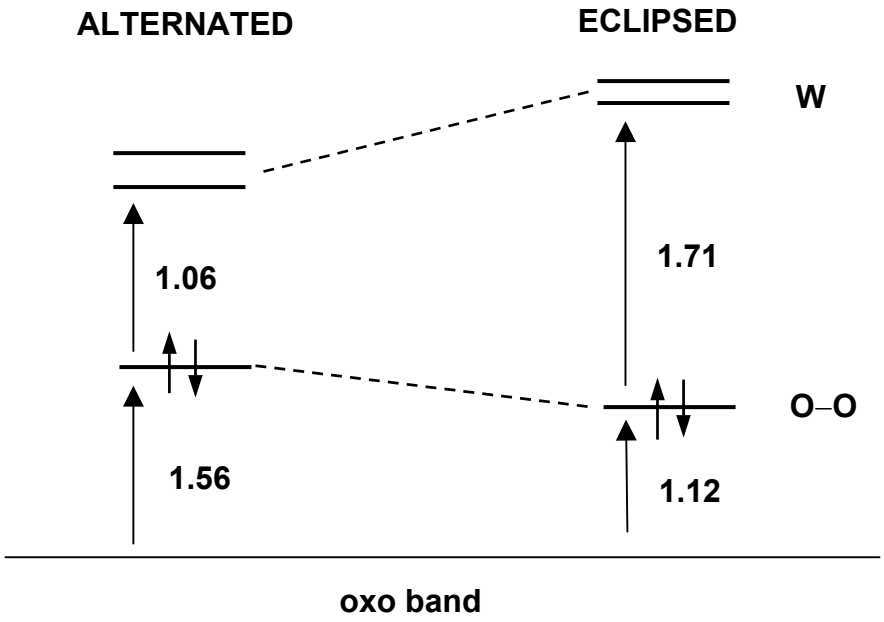

Figure 6.16. Relative frontier orbitals energies (in eV) for the alternated and eclipsed peroxo $[PTiOOW_{11}O_{39}]^{5-}$ anion. See Figure 10 for a 3D representation of the HOMO in the eclipsed conformation.

According to the formal IV and VI oxidation states for Ti and W, respectively, the electronic structure of $[P(TiO_2)W_{11}O_{39}]^{5-}$ is characterised by two sets of orbitals relatively close in energy. The HOMO in the non-protonated species is fairly localised over the O–O group, and the empty set of d-metal orbitals appear 1.71 eV above the occupied band at the DFT level, which is a somewhat small value compared to ~2.90 eV of the related $[PTiW_{11}O_{40}]^{5-}$ Keggin anion. This could be a sign of higher reactivity of the

peroxo derivative. Structures **2a** and **2b** have smaller HOMO-LUMO gaps, very close to 1.0 eV. The structure of the related $[P(WO_2)TiW_{11}O_{39}]^{5-}$ peroxo complex was computed for comparison. There are five distinct isomers according to the position of the W in relation to Ti. Since we do not expect a strong energy dependence of the cluster with the WOO position, we have arbitrarily chosen one non-neighbouring WOO–Ti form. In the eclipsed conformation for the O_2 group, the WOO complex was computed to be 13.7 kcal mol^{-1} higher in energy in relation to the most stable conformation for $[PTi(O_2)W_{11}O_{39}]^{5-}$. This important energy excludes the $[P(WO_2)TiW_{11}O_{39}]^{5-}$ peroxo complex as a result of the reaction of $[Bu_4N]_8[(PW_{11}O_{39}Ti)_2O]$ with H_2O_2.

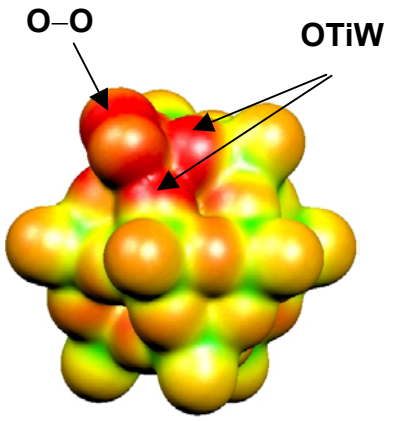

Figure 6.17. MESP function plotted over an isodensity surface for structure **2c**. Red regions represent proton-attractive sites.

A priori, the protonation of $[PTiW_{11}O_{40}]^{5-}$ could yield several isomers depending on the protonation site and the orientation of the proton. The electrostatic potential (EP) function is an useful tool in the prediction of protonation sites in a POM, allowing a qualitative classification of the relative nucleophilicity of the external regions of the POM core.[31,37] Alternatively, the protonation sites can be studied by explicit addition of protons in an attempt to find quantitative relative protonation energies.[15-16,31] Again, the relative basicity order found with the DFT methodology for several Keggin anions is in accordance with the experimental evidence.[35] In

the present case, the preferred site for protonation in $[PTi(O_2)W_{11}O_{39}]^{5-}$ was studied taking into account several isomers and orientations of the hydrogen atom. The EP function was appropriated in discriminating the most from the least favourable protonation sites in $[PTi(O_2)W_{11}O_{39}]^{5-}$.[32,35b] The EP distribution was plotted over a 3D-isodensity surface (Figure 6.17). The red colour identifies the most favourable protonation sites (nucleophilic regions). This representation suggests that the most likely positions to accept an incoming proton are the four oxygen atoms bridging the Ti and W atoms, indicated by the intense red colour in those regions. Contrarily, terminal W=O sites would be the least basic ones and, in general, the protonation in these terminal oxygens is very unlikely.[31] The O_2 group could compete in the protonation process because the EP takes similar values compared to OTiW sites.

A more quantitative description was obtained through the study of the protonated species, $[HPTi(O_2)W_{11}O_{39}]^{4-}$. When the OTiW oxygens were protonated several local minima were found. In the most stable structure A (Figure 6.18) the hydrogen is oriented towards the centre of the nearest M_4O_4 ring, a region with a high proton affinity. Notice in Figure 6.17 the intense red area nearby the M_4O_4 ring, especially in the vicinity of the OTiW sites. In structure B, the proton is equidistant from two bridging oxygens and from one of the oxygens of the peroxo group. This form is 3.7 kcal mol^{-1} above the most stable structure A in the gas phase. The relative energy of these two proton orientations changes when the solvent is included via a continuum model.[28] In acetonitrile (ε = 37.0) the two conformations are only separated by 0.4 kcal mol^{-1}. The interaction between the solvent and the anion is more efficient in structure B because the proton is oriented outwards from the anion surface.

The protonation in the peroxo ligand was also amply studied. All attempts to obtain a TiOO–H side-on coordination structure were, however, unsuccessful because the optimisation always evolved towards geometries with a η^1-coordination. This result contrast with the very recent B3LYP study of Sever and Root on the $Ti(OH)_3OOH$ model clusters, who also found structures with a η^1-coordination for the OOH group.[38]

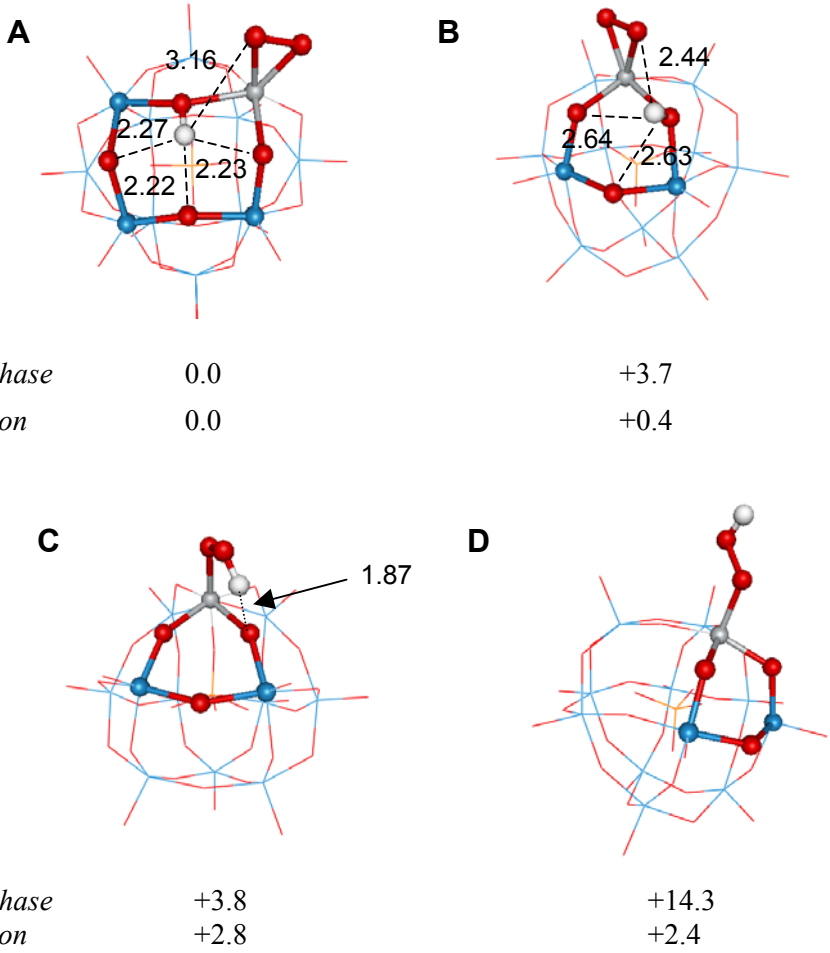

Gas phase	0.0	+3.7
Solution	0.0	+0.4

Gas phase	+3.8	+14.3
Solution	+2.8	+2.4

Figure 6.18. Optimised structures, relative energies (in kcal mol^{-1}) and H···O distances (in Å) for several isomers of $[HPTi(O_2)W_{11}O_{39}]^{4-}$. Notice the existence of a correlation between the number of H···O interactions and the stability of anion.

The larger coordination of the titanium centre in the polyoxometalate probably originates this different behaviour. The relative energy of C (Figure 6.18) in relation to A is +3.8 kcal mol^{-1} in the gas phase and only +2.8 kcal mol^{-1} in acetonitrile solution. Structure D is quite unstable, presumably due to the lack of any stabilising O···H interaction. But again, a

large stabilisation happens when the effect of the solvent is included in the calculations. In this latter case, the proton is very exposed to the solvent molecules and the relative energy for D goes from +14.3 kcal mol^{-1} in the isolated anion to only +2.4 kcal mol^{-1} in solution. Therefore, although the calculations point to OTiW as the most basic site, both H–OTiW and TiOO–H protonated anions could coexist in solution. Present calculations clearly show that, in addition to the intrinsic basicity of an oxygen site, inter and intra O···H interactions in POM clusters are of great importance in determining the protonation site in a POM.

It is worth noting that structure C (in which the O–O group has been protonated) yields the larger HOMO-LUMO gap of the series, a sign of stability of the cluster. The protonation at the peroxo ligand stabilises the energy of the HOMO, which is only 0.1 eV above the oxo band. Contrarily, the protonation in the Keggin core, as expected, does not modify the relative energy of the frontier orbitals. Finally, let us comment that the Mulliken population analysis shows a small increment of the positive charge in all the metal centres after protonation, particularly in those centres closest to the proton. Namely, the titanium atom and two of the four neighbouring W atoms. The largest change amounts 0.07 e

References and Notes

[1] Klemperer, W. G.; Shum, W. *J. Am. Chem. Soc.* **1977**, *99*, 3544.

[2] Klemperer, W. G.; Shum, W. *J. Am. Chem. Soc.* **1978**, *100*, 4891.

[3] Filowitz, M.; Ho, R. K. C.; Klemperer, W. G. *Inorg. Chem.* **1979**, *18*, 93.

[4] Besecker, C. J.; Klemperer, W. G. *J. Am. Chem. Soc.* **1980**, *102*, 7598–7600.

[5] Day, V. W.; Fredrich, M. F.; Thompson, M. R.; Klemperer, W. G.; Liu, R.-S.; Shum, W. *J. Am. Chem. Soc.* **1981**, *103*, 3597–3599.

[6] Besecker, C. J.; Klemperer, W. G.; Day, V. W. *J. Am. Chem. Soc.* **1982**, *104*, 6158–6159.

[7] Besecker, C. J.; Day, V. W.; Klemperer, W. G.; Thompson, M. R. *J. Am. Chem. Soc.* **1984**, *106*, 4125–4136.

[8] Day, V. W.; Klemperer, W. G.; Maltbie, D. J. *Organometallics.* **1985**, *4*, 104.

[9] Besecker, C. J.; Day, V. W.; Klemperer, W. G.; Thompson, M. R. *Inorg. Chem.* **1985**, *24*, 44.

[10] Day, V. W.; Klemperer, W. G.; Schwartz, C. *J. Am. Chem. Soc.* **1987**, *109*, 6030–6044.

[11] Day, V. W.; Klemperer, W. G.; Maltbie, D. J. *J. Am. Chem. Soc.* **1987**, *109*, 2991.

[12] Day, V. W.; Klemperer, W. G.; Lockledge, S. P.; Main, D. J. *J. Am. Chem. Soc.* **1990**, *112*, 2031.

[13] Day, V. W.; Klemperer, W. G.; Main, D. J. *Inorg. Chem.* **1990**, *29*, 2345–2355.

[14] Day, V. W.; Klemperer, W. G.; Main, D. J. *Inorg. Chem.* **1990**, *29*, 2355–2360.

[15] Bardin, B. B.; Bordawekar, S. V.; Neurock, M.; Davis, R. J. *J. Phys. Chem. B.* **1998**, *102*, 10817–10825.

[16] Ganapathy, S.; Fournier, M.; Paul, J. F.; Delevoye, L.; Guelton, M.; Amoureux, J. P. *J. Am. Chem. Soc.* **2002**, *124*, 7821–7828.

[17] (a) Hervé, G.; Tézé, A. *Inorg. Chem.* **1977**, *16*, 2115. (b) Massart, R.; Contant, R.; Fruchart, J. M.; Ciabrini, J. P.; Fournier, M. *Inorg. Chem.* **1977**, *16*, 2916. (c) Jeannin, Y.; Martin-Frère, J. *J. Am. Chem. Soc.* **1981**, *103*, 1664–1667. (d) Martin-Frère, J.; Jeannin, Y. *Inorg. Chem.* **1984**, *23*, 3394–3398. (e) Weakley, T. R. J. *J. Chem. Soc., Chem. Commun.* **1984**, 1406. (f) Kortz, U.; Tézé, A.; Hervé, G. *Inorg. Chem.* **1999**, *38*, 2038–

2042.

[18] Weakley, T. J. R.; Evans, H. T.; Showell, J. S.; Tourné, C. M.; Tourné, G. F. *J. Chem. Soc. Chem. Commun.* **1973**, 139. Finke, R. G.; Droege, M.; Hutchinson, J. R.; Gansow, O. *J. Am. Chem. Soc.* **1981**, *103*, 1587–1589. Evans, H. T.; Tourné, C. M.; Tourné, G. F.; Weakley, T. J. R. *J. Chem. Soc. Dalton Trans.* **1986**, 2699–2705. Finke, R. G.; Droege, M. W.; Domaille, P. J. *Inorg. Chem.* **1987**, *26*, 3886–3896. Weakley, T. J. R.; Finke, R. G. *Inorg. Chem.* **1990**, *29*, 1235–1241. Gómez-García, C. J.; Coronado, E.; Borrás-Almenar, J. J. *Inorg. Chem.* **1992**, *31*, 1667.

[19] Domaille, P. J. *J. Am. Chem. Soc.* **1984**, *103*, 7677–7687.

[20] Kempf, J. Y.; Rohmer, M.-M.; Poblet, J.-M.; Bo, C.; Bénard, M. *J. Am. Chem. Soc.* **1992**, *114,* 1136.

[21] Okuhara, T.; Mizuno, N.; Misono, M. *Adv. Catal.* **1996**, *41*, 113.

[22] Finke, R. G.; Droege, M. W. *J. Am. Chem. Soc.* **1984**, *106*, 7274–7277.

[23] Edlund, D. J.; Saxton, R. J.; Lyon, D. K.; Finke, R. G. *Organometallics.* **1988**, *7*, 1629–1704.

[24] See references 22-30 of chapter 4.

[25] Finke, R. G.; Rapko, B.; Weakley, T. J. R. *Inorg. Chem.* **1989**, *28*, 1573 and see Barnard, D. L.; Hill, C. L.; Cage, T.; Matheson, J. E.; Huffman, J. H.; Sidwell, R. W. Otto, M. I. Schinazi, R. F. *Intl. Antiviral News.* **1995**, *3*, 159–161.

[26] (a) Yamase, T.; Ozeki, T.; Sakamoto, H.; Nishiya, S.; Yamamoto, A. *Bull. Chem. Soc. Jpn*. **1993**, *66*, 103–108. (b) Lin, Y.; Weakley, T. J. R.; Rapko, B.; Finke, R. G. *Inorg. Chem.* **1993**, *32*, 5095–5101. (c) Müller, A.; Krickemeyer, E.; Dillinger, S.; Meyer, J.; Bögge, H.; Stammler, A. *Angew. Chem., Int. Ed. Engl.* **1996**, *35*, 171–173. (d) Kim, G.-S.; Zeng, H.; Rhule, J. T.; Weinstock, I. A.; Hill, C. L. *J. Chem. Soc., Chem. Commun.* **1999**, 1651–1652. (e) Kim, G.-S.; Zeng, H.; VanDerveer, D.; Hill, C. L. *Angew. Chem., Int. Ed. Engl.* **1999**, *38*, 3205–3207.

[27] Kholdeeva, O. A.; Maksimov, G. M.; Maksimovskaya, R. I.; Kovaleva, L. A.; Fedotov, M. A.; Grigoriev, V. A.; Hill, C. L. *Inorg. Chem.* **2000**, *39*, 3828–3837.

[28] Pye, C. C.; Ziegler, T. *Theor. Chem. Acc.* **1999**, *101*, 396. ADF 2000.01. Department of Theoretical Chemistry. Vrije Universiteit. Amsterdam. Baerends, E. J.; Ellis, D. E.; Ros, P. *Chem. Phys.* **1973**, *2*, 41. Versluis, L.; Ziegler, T. *J. Chem. Phys.* **1988**, *88*, 322. Te Velde, G.; Baerends, E. J. *J. Comput. Phys.* **1992**, *99*, 84. Fonseca Guerra, C.; Snijders, J. G.; Te Velde, G.; Baerends, E. J. *Theor. Chem. Acc.* **1998**, *99*, 391.

[29] Kholdeeva, O. A.; Maksimovsaya, R. I.; Maksimov, G. M.; Zamarev, K. I. *React. Kinet. Catal. Lett*. **1998**, *63*, 95.

[30] Kim, G.-S.; Zeng, H.; Cowan, J. J.; Neiwert, W. A.; VanDerveer, D.; Hill, C. L.; Weinstock, I. A. *Inorg. Chem.* **2003**, *42*, in press.

[31] López, X.; Bo, C.; Poblet, J. M. *J. Am. Chem. Soc.* **2002**, *124*, 12574.

[32] Maestre, J. M.; Sarasa, J. P.; Bo, C.; Poblet, J. M. *Inorg. Chem.* **1998**, *37*, 3071.

[33] Manuscript in preparation.

[34] Sheldon, R. A.; Kochi, J. K. *Metal-Catalyzed Oxidations of Organic Compounds,* Academic Press, New York, **1981**. Sheldon, R. A.; Dakka, J. *Catal. Today.* **1994**, *19*, 215. Notari, B. *Adv. Catal.* **1996**, *41*, 253. Centi, G.; Misono, M. *Catal. Today* **1998**, *41*, 287. Clerici, M. G. *Topics in Catalysis* **2000**, *13*, 373. Sanderson, W. R. *Pure and Appl. Chem.* **2000**, *72*, 1289. Arends, I. W. C. E.; Sheldon, R. A. *Appl. Catal. A: General.* **2001**, *212*, 175.

[35] (a) Poblet, J. M.; López, X.; Bo, C. *Chem. Soc. Rev.* **2003**, 297; (b) Rohmer, M.-M.; Bénard, M.; Blaudeau, J.-P.; Maestre, J. M.; Poblet, J. M. *Coord. Chem. Rev.* **1998**, *178–180*, 1019.

[36] López, X.; Maestre, J. M.; Bo, C.; Poblet, J. M. *J. Am. Chem. Soc.* 2001, **123***,* 9571.

[37] Maestre, J. M.; López, X.; Bo, C.; Casañ-Pastor, N.; Poblet, J. M. *J. Am. Chem. Soc.* **2001**, *123*, 3749. Bridgeman, A. J.; Cavigliasso, G. *Inorg. Chem.* **2002**, *41*, 1761. Bridgeman, A. J.; Cavigliasso, G. *Inorg. Chem.* **2002**, *41*, 3500.

[38] Sever, R. R.; Root, T. W. *J. Phys. Chem*. **2003**, *107*, 4090